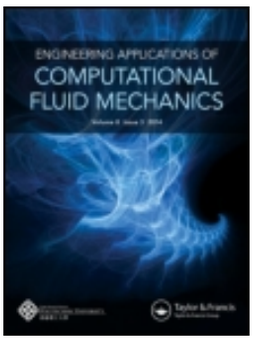

Taylor & Francis
Taylor & Francis Group

Engineering Applications of Computational Fluid Mechanics

ISSN: 1994-2060 (Print) 1997-003X (Online) Journal homepage: http://www.tandfonline.com/loi/tcfm20

CFD simulation of a turbulent fiber suspension flow – a modified near-wall treatment

Carla Cotas, Dariusz Asendrych, Fernando Garcia, Pedro Faia & Maria Graça Rasteiro

To cite this article: Carla Cotas, Dariusz Asendrych, Fernando Garcia, Pedro Faia & Maria Graça Rasteiro (2015) CFD simulation of a turbulent fiber suspension flow – a modified near-wall treatment, Engineering Applications of Computational Fluid Mechanics, 9:1, 233-246, DOI: 10.1080/19942060.2015.1005872

To link to this article: https://doi.org/10.1080/19942060.2015.1005872

Published online: 02 Mar 2015.

Engineering Applications of Computational Fluid Mechanics, 2015
Vol. 9, No. 1, 233–246, http://dx.doi.org/10.1080/19942060.2015.1005872

Taylor & Francis
Taylor & Francis Group

CFD simulation of a turbulent fiber suspension flow – a modified near-wall treatment

Carla Cotas[a], Dariusz Asendrych[b], Fernando Garcia[a], Pedro Faia[c] and Maria Graça Rasteiro[a]*

[a]*Chemical Engineering and Forest Products Research Centre (CIEPQPF), Chemical Engineering Department, Faculty of Sciences and Technology, University of Coimbra, Rua Sílvio Lima, Pólo II, 3030-790 Coimbra, Portugal;* [b]*Częstochowa University of Technology, Institute of Thermal Machinery, 42-200 Częstochowa, Poland;* [c]*Electrical and Computers Engineering Department, Faculty of Sciences and Technology, University of Coimbra, Portugal*

(*Received 11 July 2014; final version received 7 January 2015*)

Turbulent *Eucalyptus* fiber suspension flow in pipes was studied numerically using commercial CFD software. A pseudo-homogeneous approach was proposed to predict the flow behavior of pulp fiber suspensions for medium consistencies and for Reynolds numbers ranging from $4.7 \div 65.3 \cdot 10^3$. Viscosity was introduced into the model as a function of shear rate to represent the non-Newtonian behavior of the pulp suspension. Additionally, the existence of a water annulus was considered at the pipe wall, surrounding the flow core, where viscosity is equal to the water viscosity. The near-wall treatment was modified considering an expression for the logarithmic velocity profile in the boundary layer, similar to the one suggested by Jäsberg (2007). The final model could reproduce the drag-reduction effect resulting from the presence of fibers in the flow. Moreover, the numerical results show that a better fit for pressure drop is obtained when the modified near-wall treatment is used and the Jäsberg adjustable parameters are adapted to take into account the flow conditions.

Keywords: turbulent pulp fiber flow; k-ε turbulence model; near-wall treatment modification; computational fluid dynamics; drag reduction; water annulus

1. Introduction

The flows of pulp fiber suspensions are important in the papermaking industry. The properties of the final product can be different depending on the characteristics of the pulp in the pipes. Furthermore, in different stages of the process an incorrect design of the flow system can lead to an inefficient operation of a pump and to excessive energy consumption. In pulp and paper mills, the design of most process equipment still remains based on empirical correlations that can fail when the process conditions change. There is currently great interest in the experimental and numerical studies of pulp suspension flows as they still remain poor and incomplete. The design of pulp and paper process equipment can be improved by using computational tools, such as, CFD (computational fluid dynamics) methods. Their use requires, however, the input knowledge necessary to develop the numerical models.

The final product in the papermaking industry can be directed for particular applications and be quite different, but the manufacturing processes are basically the same. The chemistry, physics and fluid dynamics are the main important areas of knowledge, in this process (Lundell et al., 2011). However, fiber suspensions are different and more complex than the other solid-liquid systems due to complex interactions between the different pulp and paper components (Ventura et al., 2008).

Three main groups can be distinguished in the fluid mechanics related to the paper making process: (*i*) the modelling of fiber suspensions, (*ii*) experimental methods to obtain the data necessary for tuning and validation of the models, and (*iii*) the knowledge about the coupling between rheology and suspension characteristics (e.g., fiber length, morphology, and concentration) (Lundell et al., 2011).

At the rheological level, the pulp fiber suspension behavior is peculiar and, there are different situations where the flow regimes and pressure loss curves are different from those of typical slurry or Newtonian liquid flow systems. When the shear stress exceeds the yield stress, τ_y, the flow of pulp suspension starts (Figure 1) (Ventura et al., 2007). When the shear stress exerted on the mass of fibers surpasses the fluidization point, τ_d, the network structure becomes totally disrupted and the suspension starts to exhibit a fluid-like behavior (Ventura et al., 2007). At this point, the suspension begins to move in a fully developed turbulent pipe flow with its hydrodynamic properties similar to those of water.

The existing studies report three different regimes in the flow of pulp fiber suspensions: plug, transition and turbulent flow regimes (Figure 2). The flow regimes are different from those for Newtonian fluids or even for other solid suspensions. In each regime there are also sub-regimes

*Corresponding author. Email: mgr@eq.uc.pt

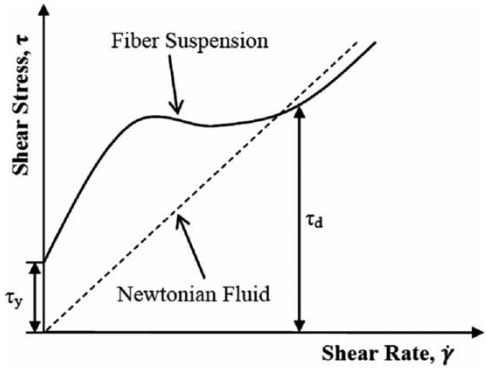

Figure 1. Stress versus shear rate curve for a fibre suspension (adapted from Gullichsen & Härkönen (1981)).

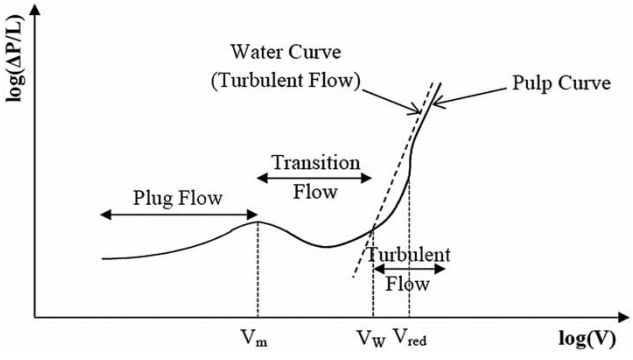

Figure 2. Typical pressure drop curve for pulp suspensions (adapted from Lundell et al. (2011) and Li et al. (2001)).

reported in literature with well-defined shear mechanisms (Fock et al., 2009; Gullichsen & Härkönen, 1981; Ventura et al., 2008). Initially, a plug of fibers is in contact with the pipe wall without any movement, a shear force has to strain the plug and when the yield stress is exceeded the motion begins. At low velocities, the suspension flows as a plug of fibers and water which induces larger values of pressure drop than those for water flow in a pipe. V_m is the velocity corresponding to the maximum of the head loss curve at the plug flow. At high velocities, the pressure loss is lower than the expected for water and all the components are in complex turbulent motion (Ventura et al., 2008). In the transition regime corresponding to intermediate velocities, a turbulent fiber-water annulus surrounds an intact plug. The transition flow regime starts at the velocity V_m (Ventura et al., 2008). The fiber plug size decreases and the turbulence intensity grow with the increase of velocity and more fibers leave the plug. The whole suspension shows a turbulent-like behavior when the velocity exceeds the point where the fiber suspension and water flow curves intersect and become parallel. V_W represents the velocity corresponding to the onset of drag reduction (Ventura et al., 2008) and V_{red} stands for the speed corresponding to the maximum of drag-reduction effect.

The simulation of pulp fiber suspension flows is a recent topic and different models with different complexity levels have been proposed to describe such flows – the pseudo-homogeneous models and the multiphase models, each having a specific domain of application. The modeling strategies which can be employed to simulate papermaking flows are extensively discussed in Hämäläinen et al. (2011). The multiphase models are only appropriate for dilute systems while the pseudo-homogeneous models are suited for concentrated systems. The implementation of the mathematical models to simulate the flow of suspensions with high consistency and high Reynolds numbers can be difficult due to the high computer requirements. In fact, simulation of the fiber suspension flows encounters various problems. Among the most important difficulties it must be mentioned the measurement of suspension apparent viscosity and yield stress (Blanco et al., 2007). Moreover, the heterogeneous mass distribution and formation of depletion layers at flow boundaries (Derakhshandeh et al., 2011) should be taken into account for the successful simulation. Some authors also emphasize the viscoelastic behavior of pulp suspensions which may have impact on the flow modeling (Derakhshandeh et al., 2011; Huhtanen & Karvinen, 2005). The successful example of CFD application to model the pulp suspension flows in various geometries (pipe, converging channel, mixing tank) with the use of single-phase approach is presented in the work of Huhtanen & Karvinen (2005). In order to simulate the drag-reduction effect in the pipe flow due to reduced fiber concentration in the near-wall region they applied the slip boundary condition at the wall. They also tested various non-Newtonian pulp models and found power-law fluid model as the most adequate for turbulent regime. Their findings were confirmed by experimental trials (Huhtanen & Karvinen, 2006). Hammarström (2004) proposed a single-phase continuum model based on his experimental observation by combining the conventional fluid dynamics law, non-Newtonian behavior and turbulence. He also considered the existence of the lubrication layer between the flow core and the pipe wall behaving in Newtonian manner. The works of Huhtanen & Karvinen (2006) and Hammarström (2004) show, however, that successful modeling requires deep knowledge about the fiber properties including their dimensions, surface quality and process history and each simulation requires special care and use of individually determined constants.

The continuum model was also shown to be an adequate tool to reconstruct the unsteady pulp flow in an LC refiner (Kondora & Asendrych, 2013), characterized by the system of spiral secondary flows. Additionally, CFD methods were applied successfully to study the flow of other fluids. The steady state swirling flow in draft tubes was studied by applying k-ε turbulence models (Galván et al., 2011) considering the wall function and a near-wall treatment to model the near-wall region. Solid suspension

flow in a cylindrical stirred tank equipped with four side-entering impellers was modeled using CFD models (Fang et al., 2013). A CFD study concerning the turbulent flow of nanofluids over periodic rib-grooved channels is presented in Vatani & Mohammed (2013).

The present study is focused on a mathematical model capable of describing properly the turbulent pipe flow of *Eucalyptus* pulp fibers. The numerical study was made using commercial CFD code with implemented modifications to the built-in model enabling to take into account the presence of fibers in the flow. It applies a pseudo-homogeneous one-phase approach that is appropriate for concentrated fiber suspensions. The classical near-wall model assuming the logarithmic velocity profile was extended by an additional term being dependent on the pulp suspension properties according to the idea of Jäsberg (2007). Moreover, the water annulus free of fibres was assumed to bound the flow core. In this way the inhomogeneity of the suspension in the wall vicinity could be captured, where fiber concentration falls down reaching zero at the wall (Dong et al., 2003). The viscosity of the water annulus is that of water, thus leading to significant reduction of flow resistance. The model validation was made by comparing the numerically obtained pressure drops with experimental data acquired at the reference pilot rig for the same flow conditions (Ventura et al., 2008) and pulp properties (Ventura et al., 2007). The paper is organized in 5 Sections. The current Section introduces the subject of the work, the general concepts and its main objectives. Section "Experimental data" reports the experimental information used in this study. Section "Numerical methodology" describes the mathematical model and the numerical scheme used to simulate the turbulent pipe flow of *Eucalyptus* pulp fibers. Section "Results and discussion" presents the results obtained with the proposed model and provides their interpretation. Section "Conclusions" summarizes the most relevant and important outcomes of this work.

2. Experimental data

The turbulent pipe flow of an *Eucalyptus* pulp (fiber averaged length of 0.706 mm (Ventura et al., 2007, 2008)) was simulated for different experimental flow rates and fiber consistencies. The correlations and data to be introduced in the CFD code were obtained from experimental data (viscosity of the pulp suspensions and head loss in the pipe). This experimental information was used also to validate the mathematical model.

2.1. Rheological data

There is no standard procedure or equipment for the rheological characterization of pulp suspensions. Various off-line and in-line techniques like rotational rheometers, conventional rheometers, pipe rheometers, NMRI and UVP-PD (Fock et al., 2009) techniques can be used to acquire rheological data.

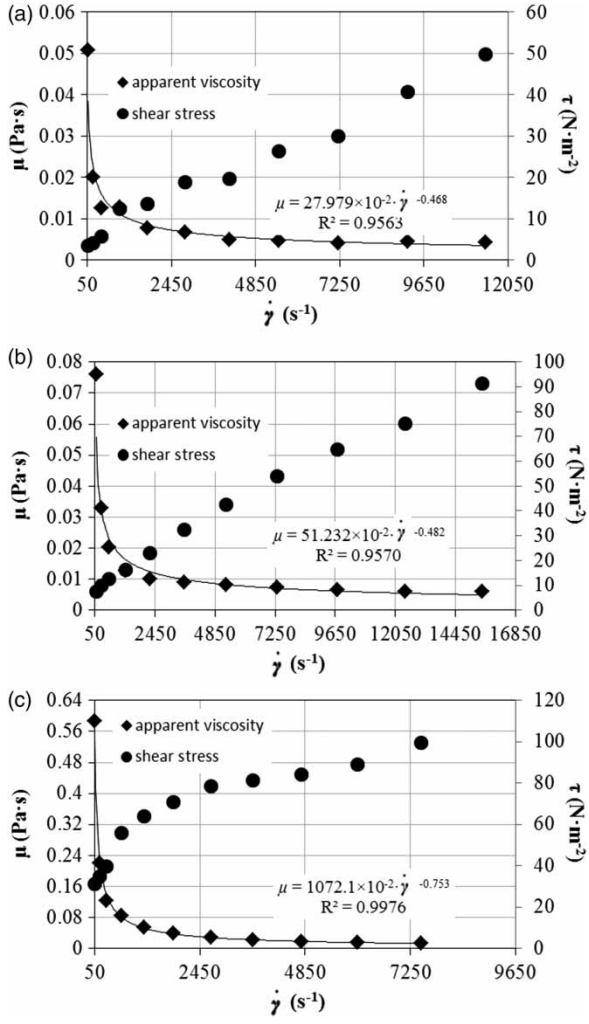

Figure 3. Rheograms and apparent viscosities for a pulp suspension of *Eucalyptus* fibres for (a) c = 1.50%(w/w), (b) c = 1.80%(w/w), and, (c) c = 2.50%(w/w).

The rheological data (Figure 3) from literature was obtained using an off-line equipment, an adapted Searle-type rotational rheometer – plate viscometer, as described in (Blanco et al., 2007; Ventura et al., 2007). Three different *Eucalyptus* pulps with consistency equal to 1.50, 1.80, and 2.50 % (w/w) were studied.

The apparent pulp viscosity μ_{app} was regarded as a viscosity of a Newtonian fluid producing the same resistance to the flow (Ventura et al., 2011):

$$\mu_{app} = \frac{\tau}{\dot{\gamma}} \tag{1}$$

The apparent viscosity of the suspension can be expressed as a function of a shear rate by the

Non-Newtonian power-law formula:

$$\mu_{app} = K(\dot{\gamma})^{n-1} \tag{2}$$

with $n < 1$.

2.2. Flow data

The experimental data for pulp flow was adopted from Ventura et al. (2008) and Ventura et al. (2011) for velocities larger than V_{red} to insure that the Reynolds number is high enough and all the suspension are in fully developed turbulent flow. For this case the use of the standard k-ε turbulence model is appropriate (Reynolds number varied between $4.7 \div 65.3 \cdot 10^3$). These data were acquired in a pilot rig properly adapted to study pulp suspension flows. The main information from literature was the pressure drop used to validate the numerical simulations.

The test section in the pilot rig is composed of a horizontal pipe 11.5-m long and 0.0762 m in diameter (Ventura et al., 2008). The flow section system is equipped with an electromagnetic flowmeter, a differential pressure transducer and a thermometer. The pressure taps are 4 m apart (Ventura et al., 2008). An appropriate (4 m) entrance length ensures that the flow is fully developed inside the test section. Downstream that section a sufficiently long pipe segment guarantees that the exit effects can be neglected.

3. Numerical methodology

3.1. Governing equations

The basic configuration of the flow domain is schematically represented in Figure 4. The *Eucalyptus* pulp is supplied into the pipe through the inlet section at the left and leaves it through the outlet section at the right. The pipe walls were assumed to be smooth. Pipe dimensions, i.e. a diameter D and its length L, were equal to 0.0762 m and 1 m, respectively (Figure 4). The length of the pipe could be reduced with respect to the test section used in the experiment, as the flow was assumed to be fully developed turbulent pipe flow.

The flow was assumed to be: (*i*) steady state, (*ii*) isothermal, (*iii*) incompressible, (*iv*) non-Newtonian fluid, and, (*v*) 2D with axial symmetry. The extent of the numerical domain was 1 m × 0.0381 m (*length* × pipe *radius*).

The dynamic viscosity of the *Eucalyptus* pulp was expressed by Equation (2) considering it as a function of local shear rate expressed by a power-law formula. The pulp density was considered equal to water density since the density of water and *Eucalyptus* pulp are very similar. The numerical methodology used was based on the solution of the partial differential equations governing the transport phenomena in a single fluid motion – the mass and the momentum conservation equations. In this study, the two-layer standard high Reynolds k-ε turbulence model was used. Therefore, two additional transport equations for the turbulent kinetic energy (k) and its dissipation rate (ε) were considered to create a complete system of governing equations to be solved (ANSYS FLUENT, 2011; Chang et al., 1995; Hsieh & Chang, 1996; Mathur & He, 2013):

Mass Conservation Equation

$$\frac{\partial u}{\partial x} + \frac{\partial v}{\partial r} + \frac{v}{r} = 0 \tag{3}$$

Axial Momentum Conservation Equation

$$\begin{aligned} &\frac{1}{r}\left[\frac{\partial}{\partial x}(r\rho uu) + \frac{\partial}{\partial r}(r\rho vu)\right] \\ &\quad = -\frac{\partial p}{\partial x} + \frac{1}{r}\left[\frac{\partial}{\partial x}\left(r(\mu+\mu_t)\frac{\partial u}{\partial x}\right) + \frac{\partial}{\partial r}\left(r(\mu+\mu_t)\frac{\partial u}{\partial r}\right)\right] \\ &\quad + \frac{\partial}{\partial x}\left[(\mu+\mu_t)\frac{\partial u}{\partial x}\right] + \frac{1}{r}\frac{\partial}{\partial r}\left[r(\mu+\mu_t)\frac{\partial v}{\partial x}\right] \end{aligned} \tag{4}$$

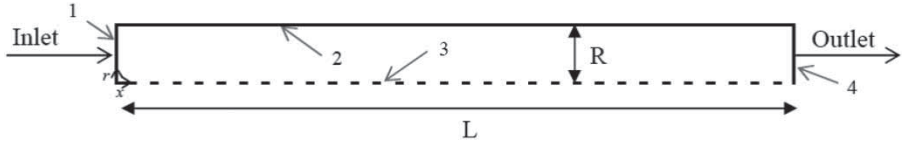

L (m)	R (m)
1	0.0381

Location	Boundary Conditions
Left side –1	Periodic boundary
Right side -4	
Top –2	Wall
Bottom -3	Axis

Figure 4. Numerical domain and boundary conditions applied.

Radial Momentum Conservation Equation

$$\frac{1}{r}\left[\frac{\partial}{\partial x}(r\rho uv)+\frac{\partial}{\partial r}(r\rho vv)\right] = -\frac{\partial p}{\partial r}+\frac{1}{r}\left[\frac{\partial}{\partial x}\left(r(\mu+\mu_t)\frac{\partial v}{\partial x}\right)+\frac{\partial}{\partial r}\left(r(\mu+\mu_t)\frac{\partial v}{\partial r}\right)\right] + \frac{\partial}{\partial x}\left[(\mu+\mu_t)\frac{\partial u}{\partial r}\right]+\frac{1}{r}\frac{\partial}{\partial r}\left[r(\mu+\mu_t)\frac{\partial v}{\partial r}\right] - 2(\mu+\mu_t)\frac{v}{r^2} \quad (5)$$

Turbulent Kinetic Energy Conservation Equation

$$\frac{1}{r}\left[\frac{\partial}{\partial x}(r\rho uk)+\frac{\partial}{\partial r}(r\rho vk)\right] = \frac{1}{r}\left[\frac{\partial}{\partial x}\left(r\left(\mu+\frac{\mu_t}{\sigma_k}\right)\frac{\partial k}{\partial x}\right)+\frac{\partial}{\partial r}\left(r\left(\mu+\frac{\mu_t}{\sigma_k}\right)\frac{\partial k}{\partial r}\right)\right] + \mu_t\left\{2\left[\left(\frac{\partial u}{\partial x}\right)^2+\left(\frac{\partial v}{\partial r}\right)^2+\left(\frac{v}{r}\right)^2\right]+\left(\frac{\partial v}{\partial x}+\frac{\partial u}{\partial r}\right)^2\right\} - \rho\varepsilon \quad (6)$$

Dissipation Rate of Turbulent Kinetic Energy Conservation Equation

$$\frac{1}{r}\left[\frac{\partial}{\partial x}(r\rho u\varepsilon)+\frac{\partial}{\partial r}(r\rho v\varepsilon)\right] = \frac{1}{r}\left[\frac{\partial}{\partial x}\left(r\left(\mu+\frac{\mu_t}{\sigma_\varepsilon}\right)\frac{\partial \varepsilon}{\partial x}\right)+\frac{\partial}{\partial r}\left(r\left(\mu+\frac{\mu_t}{\sigma_\varepsilon}\right)\frac{\partial \varepsilon}{\partial r}\right)\right] + C_{\varepsilon 1}\mu_t\frac{\varepsilon}{k}\left\{2\left[\left(\frac{\partial u}{\partial x}\right)^2+\left(\frac{\partial v}{\partial r}\right)^2+\left(\frac{v}{r}\right)^2\right]+\left(\frac{\partial v}{\partial x}+\frac{\partial u}{\partial r}\right)^2\right\} - C_{\varepsilon 2}\frac{\varepsilon^2}{k} \quad (7)$$

The turbulence model constants σ_k, σ_ε, $C_{\varepsilon 1}$ and $C_{\varepsilon 2}$ were assumed to be equal to their standard values (Ferziger & Peric, 2002). The turbulent viscosity being a feature of the flow was locally computed by combining k and ε as follows (Ferziger & Peric, 2002):

$$\mu_t = \rho C_\mu \frac{k^2}{\varepsilon} \quad (8)$$

where C_μ is equal to 0.09.

3.2. Numerical solution procedure

The system of partial differential Equations (3) to (7) consists of non-linear equations and includes derivative terms of first and second order in space. The equations are discretized by a finite volume method (Ferziger & Peric, 2002). The differential equations are integrated for each individual control volume in the computational domain to deduce the algebraic equations for the unknown discrete variables that can be solved numerically. The linearization of discretized equations results in a linear system of equations and its solution provides updated values for the dependent variables. A second-order upwind scheme was selected to interpolate the face values required for the convection terms in the discretized equations of dependent variables from cell centre values, i.e., it is assumed that the quantities of variables at cell faces are similar to the values in the cell centre that represents a cell-average value. The cell face variable value is equal to the variable value in the cell centre in the upstream cell (Ferziger & Peric, 2002). A pressure equation is solved by manipulating the continuity and momentum equations to extract the pressure field, with the use of the pressure-based approach. The SIMPLE algorithm was chosen to obtain the pressure field (Ferziger & Peric, 2002). An additional condition for the pressure was derived by reformulating the continuity equation and the mass conservation was implemented using a relationship between velocity and pressure corrections.

The mesh used for the computational domain is a uniform mesh with 20 × 54 nodes, according to x and r coordinates, respectively. The total number of cells is equal to 1007 and the number of faces is 2033. The number of iterations considered for the periodic boundary condition is equal to 2 and the relaxation factor equal to 0.5. Numerical tests showed that the mesh selected for this study gives grid-independent solutions for all investigated cases. The first mesh node is placed at $y^+ > 30$ (fully turbulent region) as recommended for the cases where wall functions are used (Xu & Aidun, 2005). The convergence criterion of the iterative process is that the residuals of all equations were less than 10^{-5}.

3.3. Boundary conditions

Boundary conditions are required for the numerical solution of the complete system of equations. The boundary conditions in the present study are related to the inlet flow (1), outlet flow (4), pipe wall (2), and pipe axis (3) (see Figure 4).

The boundary conditions for inlet and outlet sections were specified as periodic boundary conditions. The turbulent pulp flow can be regarded as a periodic flow due to the periodicity of both, the physical geometry and expected pattern of the flow. The periodic boundary condition selected for the cases studied was the pressure-drop periodic flow in which a pressure drop is present across the translational periodic boundary and the flow is regarded as "fully developed" flow. The data to be reproduced numerically were obtained in a pipe section located 4-m downstream an entrance region ensuring fully developed flow. The periodic boundary conditions selected allow the simulation of pipe segment 1-m long, specifying the mass flow rate to each case and to obtain the pressure gradient to compare with the experimental pressure value.

Along the flow direction the flow quantities are periodic (Ferziger & Peric, 2002), which can be expressed as:

$$\frac{\partial(\bullet)}{\partial x} = 0 \tag{9}$$

except the pressure which drops linearly

$$\frac{\partial p}{\partial x} = const \tag{10}$$

The periodic boundary conditions mean that there is no need to specify the turbulence parameters at the inlet boundary which will be computed in all domain to satisfy the flow governing equations. As referred previously the only physical setting specified is the mass flow rate.

The main objective of the present work is to analyze the influence a modified near-wall treatment has on the prediction of the turbulent pipe flow of pulp fibres suspensions. Ventura et al. (2011) adjusted the turbulence parameters according to the pulp consistency, here the authors focused on the modification of the near wall treatment. A future study will be performed to analyze the influence of both the modified near-wall treatment and turbulence quantities supplied in the inlet section which should be considered as *velocity inlet* or *mass flow inlet* instead of the present *periodic* boundary condition.

The following boundary conditions were applied in the model. At the pipe symmetry axis, the axis boundary condition type was set. The wall boundary condition was selected for the boundary representing the pipe wall, where the no-slip condition was chosen for velocity ($u_{Wall} = v_{Wall} = 0$). The shear stress on the pulp at the wall is predicted, in ANSYS FLUENT 13.0, using the properties of the flow adjacent to the wall boundary (ANSYS FLUENT, 2011) considering the momentum wall functions. The near-wall region was modeled with the use of the wall function approach. In this approach, the viscous sublayer is not resolved and wall functions are used to bridge the viscosity affected region. The wall law for mean velocity was modified according to the expressions presented in Jäsberg (2007). The boundary condition for k imposed at the wall is (ANSYS FLUENT, 2011):

$$\left.\frac{\partial k}{\partial n}\right|_{Wall} = 0 \tag{11}$$

The k dissipation rate equation is not solved at the wall-adjacent cells, it is assumed to be equal in the wall-adjacent control volume, computed at the first near-wall point P from (ANSYS FLUENT, 2011):

$$\varepsilon_P = \frac{C_\mu^{3/4} \cdot k_P^{3/2}}{\kappa \cdot y_P} \tag{12}$$

where k_P and ε_P are turbulent parameters at the first near-wall node P.

At the start of the numerical calculation, the initial conditions for the field variables are specified be equal to zero except for the turbulent kinetic energy and its dissipation rate that were initialized equal to 1 $m^2 \cdot s^{-2}$ and 1 $m^2 \cdot s^{-3}$, respectively.

3.4. *Modified wall function*

A peculiar S-shaped velocity profile near the wall was experimentally observed for the pipe flow (Jäsberg, 2007) and channel flow (Xu & Aidun, 2005) of natural flexible cellulose wood fibers. In these studies, mathematical expressions were proposed for the dimensionless velocity profiles as functions of the dimensionless distance. The strategy applied in this work was to change the momentum wall law according to the expressions presented in Jäsberg (2007).

A combination of logarithmic law for the turbulent region and a wake function is presented in Xu & Aidun (2005). An expression based on the standard logarithmic velocity profile for turbulent Newtonian fluid considering three distinct regions in the fully turbulent region is proposed in Jäsberg (2007). The experimental velocity profiles were reported in Jäsberg (2007) for pine pulp suspensions (c = 1% (w/w)) and birch suspensions (c = 2% (w/w)) in a straight pipe with a sudden expansion (turbulence generator system). Figure 5 represents the dimensionless velocity profile approximation presented in Jäsberg (2007). Three distinct regions: *near wall region*, *yield region* and *core region* can be identified in the profile. In the near wall region, there is no difference between the new profile and the profile of a Newtonian flow. In the yield region, the velocity gradient is higher than that of a Newtonian flow. Last, in the core region the velocity gradient form is similar to that of a Newtonian fluid but with a lower slope.

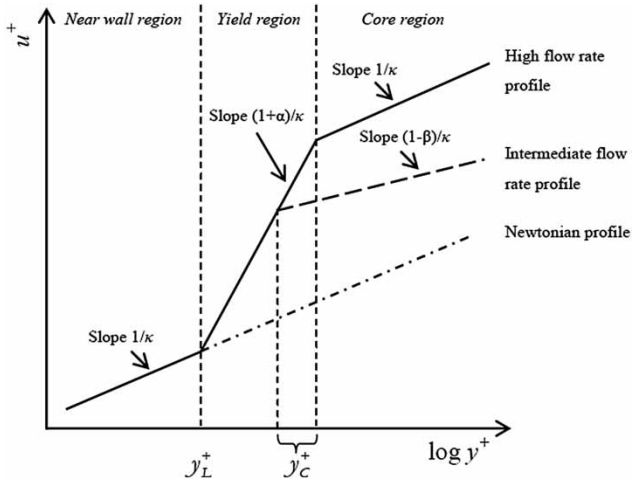

Figure 5. The structure of dimensionless velocity profile in a turbulent boundary-layer modified according to Jäsberg (2007).

Mathematically, the velocity behavior presented in Figure 5 can be expressed by Equation (13). The general expression for the dimensionless velocity profile corresponds to the *standard* logarithmic wall function modified with an additional term Δu^+, (see Equation (13)) depending on the dimensionless distance to the pipe wall and on the parameters related to the slope in the yield and core regions.

$$u^+ = \frac{1}{\kappa} ln(y^+) + \mathrm{B} + \Delta u^+ \tag{13}$$

$$\Delta u^+ = \begin{cases} 0, & 0 < y^+ < y_L^+ \\ \frac{\alpha}{\kappa}\, ln\left(\frac{y^+}{y_L^+}\right), & y_L^+ < y^+ < y_C^+ \\ \frac{\alpha}{\kappa}\, ln\left(\frac{y_C^+}{y_L^+}\right) - \frac{\beta}{\kappa}\, ln\left(\frac{y^+}{y_C^+}\right), & y_C^+ < y^+ < R^+ \end{cases} \tag{14}$$

The standard nondimensional wall-layer variables are defined as follows (Jäsberg, 2007):

$$u^+ = \frac{u}{u_\tau} \tag{15}$$

$$y^+ = \frac{\rho}{\mu_W} u_\tau y_P \tag{16}$$

$$R^+ = \frac{\rho}{\mu_W} u_\tau R \tag{17}$$

$$u_\tau = \left(\frac{\tau_W}{\rho}\right)^{1/2} \tag{18}$$

The parameters α and β are adjustable parameters that characterize the slope, in relation to the Newtonian profile value, of the envelope curve in the yield and core regions, respectively. The parameter y_L^+ represents the dimensionless distance between the near wall region and the yield region, y_C^+ indicates the variable position of the plug surface (region between the high flow rate envelope curve and the upper limit of the yield region). The standard values proposed by Jäsberg in his study for the birch pulp flow (c = 2% (w/w)) are presented in Table 1.

Table 1. *Standard* Jäsberg adjustable parameters for birch pulp flow (c = 2% (w/w)) (Jäsberg, 2007).

Parameter	α	β	y_L^+	y_C^+
Value	2.4	0.0	50	320

4. Results and discussion

The experimental conditions and flow data for which the model was applied are listed in Table 2. The non-Newtonian behavior of the *Eucalyptus* pulp was introduced into the CFD model by implementing the viscosity Equation (2) with the rheological parameters given in Table 2. The presence of a water annulus at the pipe wall surrounding the core flow was taken into account with the viscosity dramatically reduced to the water level. As shown in Asendrych & Kondora (2009) the water layer with no fibers present or with very reduced consistency leads to significant changes of the flow in the near-wall region and may have dramatic consequences to the flow resistance. The water annulus thickness was assumed equal to the mean *Eucalyptus* fiber length (0.706 mm). The *standard* law-of-the-wall for mean velocity was modified according to Equation (13). The numerical model has been validated by comparing the numerical pressure drop values with those obtained experimentally and the simulated dimensionless velocity profiles with those calculated directly using Jäsberg equation (Equation (13)).

4.1. *Standard Jäsberg adjustable parameters*

The modified law-of-the-wall for the velocity, according to Jäsberg (2007), has four parameters (Equations (13) and (14)), designated in this work as Jäsberg adjustable parameters: α, β, y_L^+ and y_C^+. The standard values proposed by Jäsberg in his study for the birch pulp flow (c = 2% (w/w)) which were presented in Table 1, were used as initial approximation in present study.

Table 2. Experimental information.

Case	c (% (w/w))	$K^{(a)}$ (Pa·s^n)	$n^{(b)}$	$U_{in}{}^{(c)}$ (m·s^{-1})	$Re_W{}^{(d)}$	$\Delta P/L_{exp.}{}^{(e)}$ (Pa·m^{-1})
A	1.50	0.2798	0.532	4.49	40170	829.1
B				6.21	65314	1288.7
C	1.80	0.5123	0.518	4.46	23847	842.6
D				6.23	38914	1203.2
E	2.50	10.721	0.247	4.90	4741	1578.9
F				5.55	6111	1753.8

(a) Consistency coefficient, Equation (2); (b) Flow behavior index, Equation (2); (c) Mean inlet *Eucalyptus* pulp flow velocity; (d) Reynolds number calculated based on the viscosity near the wall, at the interface with the water annulus (Rudman & Blackburn, 2006); (e) Experimental pressure drop value.

Table 3. Pressure drop values (cases presented in Table 1).

Case	c (% (w/w))	U_{in} [a] ($m \cdot s^{-1}$)	$\Delta P/L_{water}$ [b] ($Pa \cdot m^{-1}$)	$\Delta P/L_{exp.}$ [c] ($Pa \cdot m^{-1}$)	$\Delta P/L_{st}$ [d] ($Pa \cdot m^{-1}$)	$\Delta P/L_{num.}$ [e] ($Pa \cdot m^{-1}$)	δ [f] (%)
A	1.50	4.49	1885.2	829.1	1740.5	1324.4	59.8
B		6.21	3419.7	1288.7	3425.4	2146.9	66.6
C	1.80	4.46	1862.2	842.6	1997.1	1359.1	61.3
D		6.23	3440.0	1203.2	3545.3	2219.6	84.5
E	2.50	4.90	2212.6	1578.9	3312.8	2299.3	45.6
F		5.55	2781.1	1753.8	3741.8	2814.3	60.5

(a) Mean inlet *Eucalyptus* pulp flow velocity; (b) Only flow of water in the same pipe; (c) Experimental pressure drop value; (d) Numerical pressure drop value (standard high Reynolds k-ε turbulence model); (e) Numerical pressure drop value (high Reynolds k-ε turbulence model with modified near-wall treatment according to Jäsberg (2007) – standard values Table 1); (f) Relative error between the experimental and numerical pressure drop ($|\Delta P/L_{exp.} - \Delta P/L_{num.}|/(\Delta P/L_{exp.}) \cdot 100\%$).

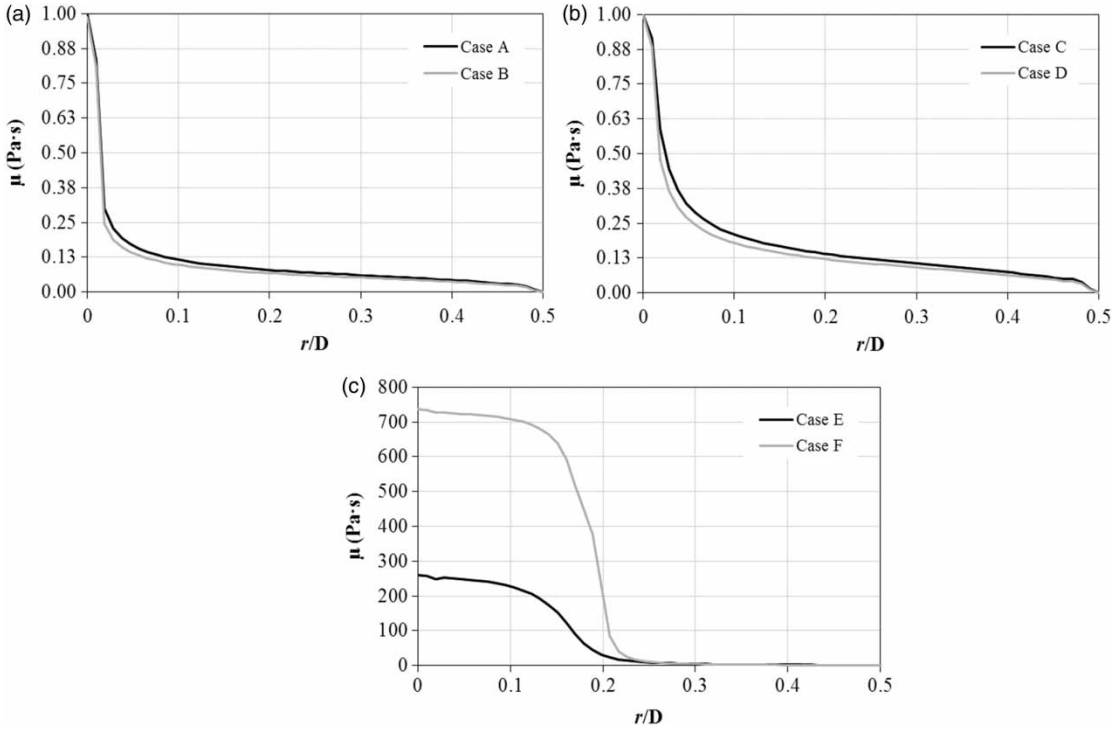

Figure 6. Numerical dynamic viscosity profiles obtained for (a) cases A and B (c = 1.50%(w/w)), (b) cases C and D (c = 1.80%(w/w)), and, (c) cases E and F (c = 2.50%(w/w)).

The numerical pressure drop results obtained with the modified CFD code are presented in Table 3 along with the experimental pressure drops for the turbulent *Eucalyptus* pulp flow and for water flow with the same bulk velocity. As expected, when the mean inlet velocity increases the pressure drop grows. The same tendency was reproduced numerically for all the cases considered. Additionally, a drag-reduction effect could always be observed in the experimental data. The numerical values are always higher than the experimental ones, showing, nevertheless the existence of drag reduction except for the highest consistency. It should be remarked, however, that the simulations were performed using the original values of Jäsberg adjustable parameters presented in Table 1. As in Jäsberg (2007) birch fiber suspension was investigated, this fibers having different properties compared with eucalyptus fibers even if length is similar, that can be the reason for the behavior discrepancies between experimental and simulation results. However, this approach is better to simulate the turbulent pulp flow under study than the standard high Reynolds k-ε turbulence model (Equation (13) considering $\Delta u^+ = 0$) which results on pressure drop values closer to those obtained only when flow of water is considered in the same pipe geometry (see Table 3), thus indicating the presence of a drag reduction effect.

In the tests with *Eucalyptus* pulp of consistency equal to 2.50% (cases E and F), it was expected that the viscosity values should be higher than those for the other two lower consistencies and, also, a higher viscosity gradient would occur across the pipe. Probably, in these cases, a wider core region and higher velocity gradients in the yield region should be expected, corresponding to a higher value for the Jäsberg adjustable parameter α and a lower value for y_C^+ than the standard one.

In this work, the complete set of differential equations was modified by introducing the non-Newtonian behavior of pulp – modification of the diffusion term of differential equations. The dynamic viscosity is a parameter to take into account in the discussion of the results. Dynamic viscosity profiles for the cases reported in Table 3 are presented in Figure 6. In all the cases, the viscosity reaches its maxima in the centre of the pipe and decreases toward the pipe wall, where no fibers are present, resulting in very low flow resistance. A more uniform radial distribution of fibers is present when the fiber consistency is lower and the total number of fibers in the flow is also lower. For the highest consistency, the viscosity profile observed in Figure 6(c) expresses the higher resistance to the flow in the central region of the pipe reflecting the high concentration of fibers forming the core region.

The large difference in the viscosity ranges between the cases in which the pulp consistency is equal to 2.50% (w/w) and cases in which it is equal to 1.50 and 1.80 % (w/w), observed in Figure 6, is in agreement with the difference in viscosity ranges observed in Figure 3 obtained experimentally. The difference in the scales of viscosity between the corresponding cases from Figure 3 and Figure 6 can be due to the fact that the experimental rheological data are not available for shear rates lower than 50 s^{-1} where it is observed the tendency to have a very high variation in viscosity as a function of shear rate. It is evident from the numerical calculations that in the centre of the pipe the shear rate attains lower values than the minimum values reached experimentally.

In Figure 7, the calculated dimensionless velocity profiles using the CFD code with the modified equations and those calculated using directly the Jäsberg Equation (13) (Jäsberg, 2007) are presented. The numerical results obtained with the modified CFD code (Equations (15) and (16)) are referred to as ModelModified, JasbergCalculation corresponds to the profile calculated with the use of Equation (13) for the dimensionless distance obtained by Equation (16). The StandardLogLaw profile designates the profiles obtained with the *standard* wall law (Equation (13) with $\Delta u^+ = 0$).

In all the cases, except when using the standard log law, the yield region and the core region can be easily identified. For the lower consistency cases (cases A to D) the dimensionless velocity profiles are closer to those calculated by

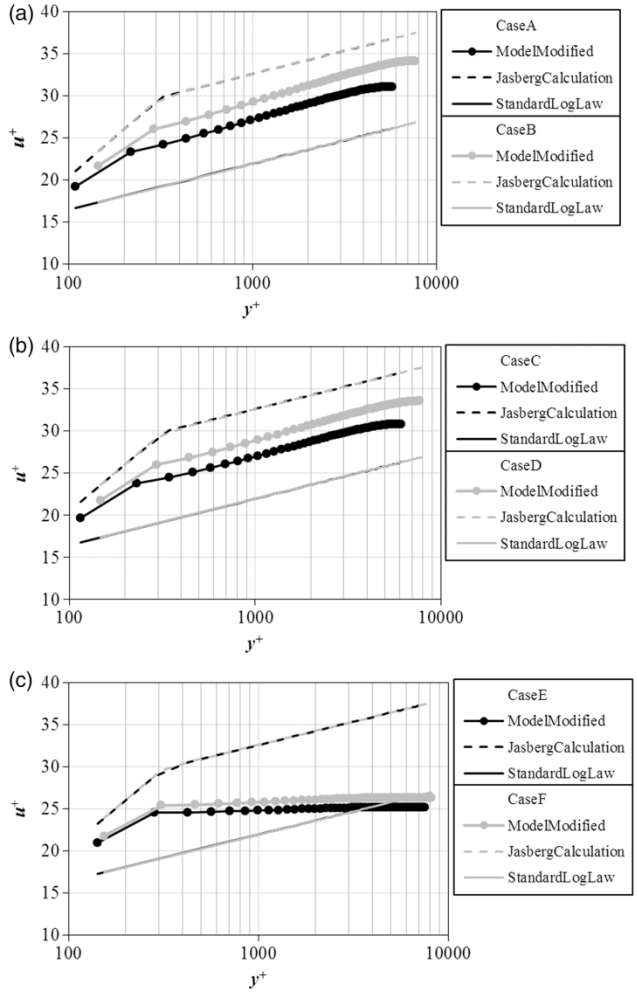

Figure 7. Dimensionless velocity profiles as a function of dimensionless distance to the pipe wall for (a) cases A and B (c = 1.50%(w/w)), (b) cases C and D (c = 1.80%(w/w)), and, (c) cases E and F (c = 2.50%(w/w)).

applying directly Equation (13). In cases E and F, an abrupt modification in the u^+ profile near the wall can be observed and it can be seen that the slope in the core region is very low. For the higher consistency cases, the diffusion term has more significance in the problem solution. Thus, the core region, where the viscosity gradient is low, presents a more uniform velocity field.

As referenced in Ventura et al. (2011), the presence of fibers in the flow creates a turbulence damping effect. Figure 8 shows the turbulent kinetic energy profiles along the pipe radius. From there, it can be concluded that when consistency increases, the turbulent kinetic energy increases, contradicting what was to be expected, but in line with the calculated pressure drop values for the highest consistency which did not reveal the existence of drag reduction. In fact, for the higher consistency it is possible that the turbulence damping region was not reached, due to pump limitations, and only tests for the transition region (see Figure 2) could be performed. In the present

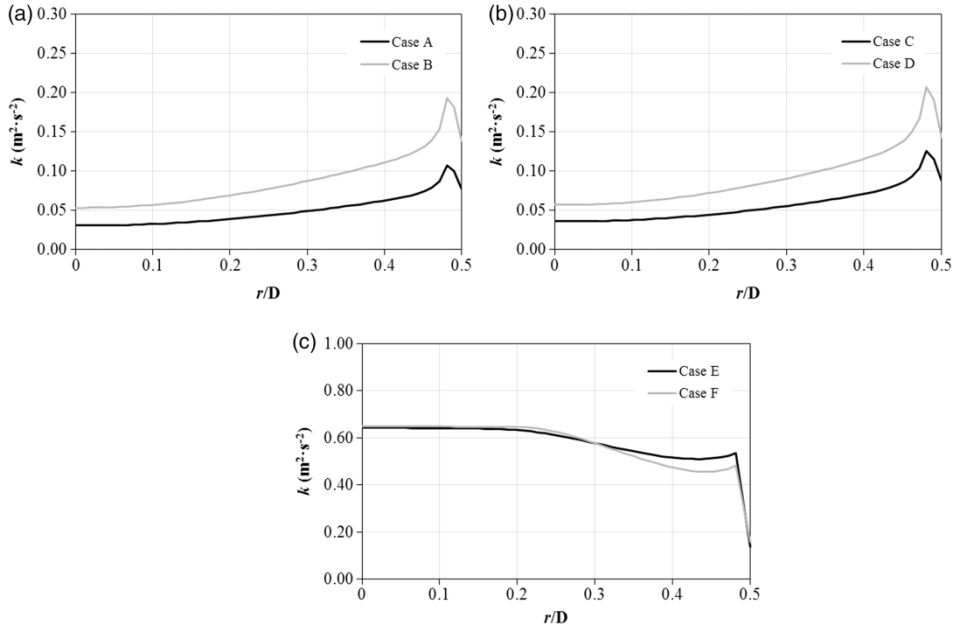

Figure 8. Numerical turbulent kinetic energy profiles for (a) cases A and B (c = 1.50%(w/w)), (b) cases C and D (c = 1.80%(w/w)), and, (c) cases E and F (c = 2.50%(w/w)).

simulation, for the lower consistency, the turbulent kinetic energy increases from the pipe axis to the pipe wall, as expected, reflecting the decrease of viscosity and increase of transverse velocity gradient towards the pipe wall. However, for the highest consistency, Figure 8.c), it can be seen that the turbulent kinetic energy for this case is higher in the pipe axis than in the pipe wall contrarily to what was expected. This behavior reflects the lower velocity gradient and dimensionless velocity gradient observed in Figure 7 for the flow of the higher consistency pulp.

These larger deviations in the turbulent kinetic energy, velocity profiles and viscosity profiles detected for the highest pulp consistency are consistent with the larger discrepancies in the pressure drop values obtained for these two cases (cases E and F). The relative errors are significant in these two cases, which is most likely due to inappropriate values of Jäsberg adjustable parameters used. So, the next step was to analyze the influence the Jäsberg adjustable parameters may have on both the dimensionless velocity profile and the corresponding pressure drop and turbulence kinetic energy profile.

4.2. *Effect of Jäsberg adjustable parameters*

The influence of the Jäsberg adjustable parameters on the dimensionless velocity profile and pressure drop was analyzed for the reference cases B, E and F (Table 4). The α parameter was increased, what corresponds physically to a larger velocity gradient in the yield region. On the other hand, the velocity gradient in the core region was considered lower by increasing β. When the velocity gradient in the yield region increases, the thickness of the core region has to increase, thus y_C^+ is reduced. For all the tests, the thickness of the near wall region was kept constant ($y_L^+ = 50$).

The pressure drop values obtained for the different cases are presented in Table 4. As discussed previously, the drag-reduction effect could not be reproduced in cases E and F. The results presented in Table 4 show that the numerical pressure drop values (*standard* Jäsberg adjustable parameters) were improved, in all cases, by modification of Jäsberg adjustable parameters. The highest improvement was achieved for the pulp consistency of 2.50% (w/w), the drag-reduction effect being now observed.

If the pulp consistency is higher, the thickness of the core region is also higher, corresponding to a lower thickness of the yield region, with a higher velocity gradient (larger slope) in this region. This effect can be seen in the velocity profiles in Figures 9 to 11. In all the cases, the presence of the yield and core regions is observed, therefore confirming the Jäsberg's predictions. The Jäsberg velocity profiles and the calculated velocity profiles become much closer when the slope of the yield region is increased (cases B1, B2, E2, E4, F2, and F4). This is more pronounced for the higher consistency where a better approximation between the calculated and experimental pressure drop was also achieved. For this consistency, the additional increase of β (flatter core region) leads to improvement in both the velocity profile and the calculated pressure drop (cases E4, F2, and F4). When the consistency increases, the increase of the plug region is expected as observed in the numerical results.

Again, as before, a higher viscosity gradient is observed when the consistency is higher (Figures 12b) and c)). In the cases of pulp consistency equal to 2.50% (w/w), the

Table 4. Different Jäsberg adjustable parameters values tested and pressure drop results.

Case	c (% (w/w))	U_{in} ($m \cdot s^{-1}$)	Parameter $y_L^+ = 50$ α	β	y_C^+	$\Delta P/L_{water}$ ($Pa \cdot m^{-1}$)	$\Delta P/L_{exp.}$ ($Pa \cdot m^{-1}$)	$\Delta P/L_{num.}$ ($Pa \cdot m^{-1}$)	δ (%)
B			2.4	0	320			2146.9	66.6
B1			3.6	0	160			1867.0	44.9
B2	1.50	6.21	3.6	0.5	160	3419.7	1288.7	1867.0	44.9
B3			4.4	0.0	100			1730.8	34.3
B4			4.4	0.9	100			1730.9	34.3
E			2.4	0	320			2299.3	45.6
E1			3.6	0	160			1888.4	19.6
E2	2.50	4.90	3.6	0.5	160	2212.6	1578.9	1840.8	16.6
E3			4.4	0.0	100			1702.6	7.8
E4			4.4	0.9	100			1602.5	1.5
F			2.4	0	320			2814.3	60.5
F1			3.6	0	160			2234.2	27.4
F2	2.50	5.55	3.6	0.5	160	2781.1	1753.8	2233.6	27.4
F3			4.4	0.0	100			2047.0	16.7
F4			4.4	0.9	100			1898.6	8.3

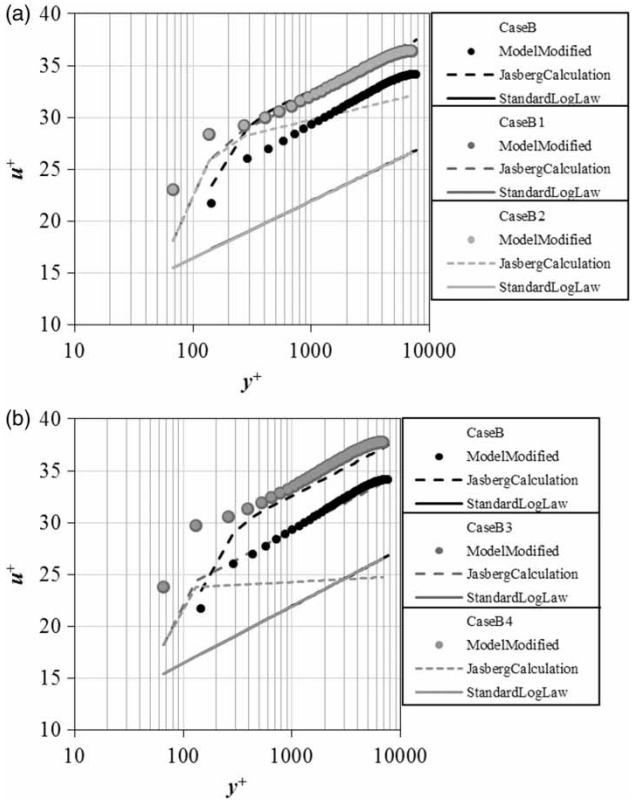

Figure 9. Dimensionless velocity profiles as a function of dimensionless distance to the pipe wall for (a) cases B, B1 and B2, and, (b) cases B, B3 and B4 (c = 1.50%(w/w), U_{in} = 6.61 $m \cdot s^{-1}$).

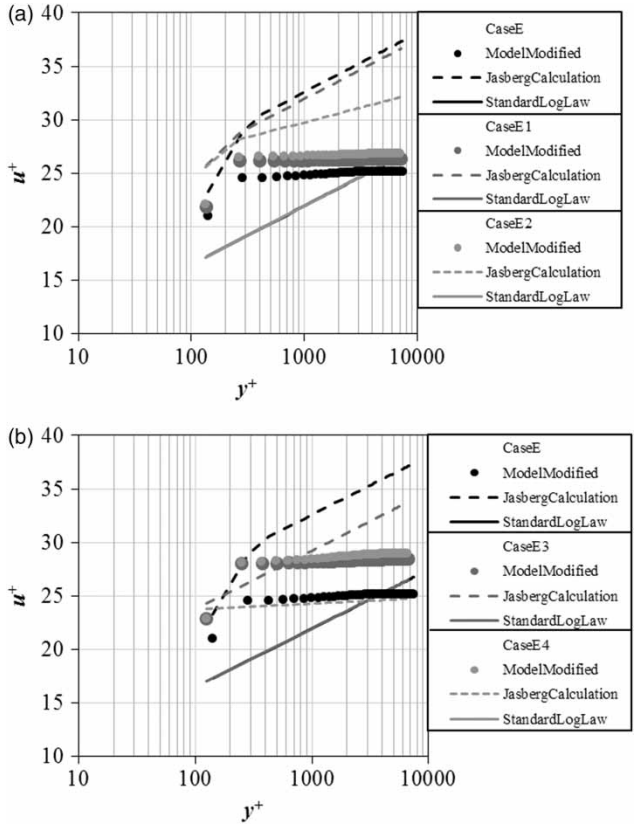

Figure 10. Dimensionless velocity profiles as a function of dimensionless distance to the pipe wall for (a) cases E, E1 and E2, and, (b) cases E, E3 and E4 (c = 2.50%(w/w), U_{in} = 4.90 $m \cdot s^{-1}$).

non-Newtonian behavior of the pulp suspension is stronger than for the lower pulp consistency studied leading to a smooth velocity gradient in the core region. Comparing the viscosity profiles obtained with the *standard* Jäsberg parameters and with the modified ones, (Figure 12) it can be observed that for the lower consistency the profiles are very similar (Figure 12a)), while for the higher consistency

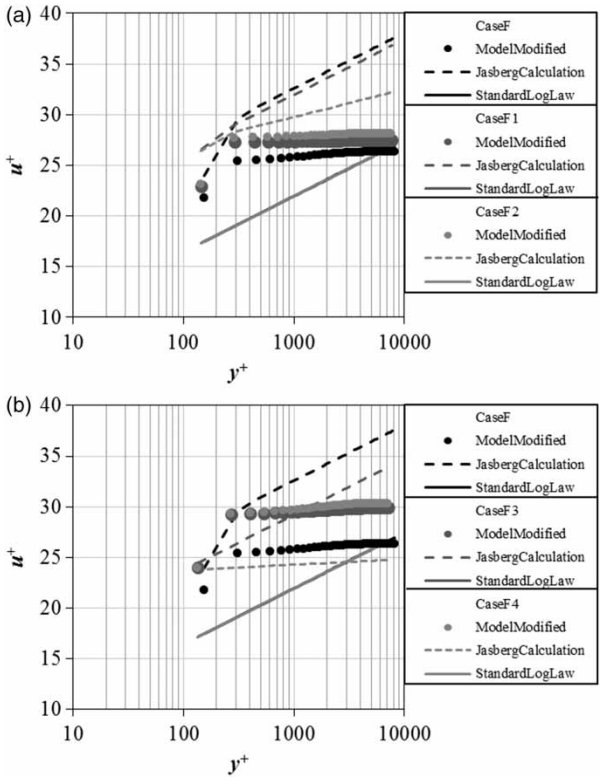

Figure 11. Dimensionless velocity profiles as a function of dimensionless distance to the pipe wall for (a) cases F, F1 and F2, and, (b) cases F, F3 and F4 (c = 2.50%(w/w), U_{in} = 5.55 m·s^{-1}).

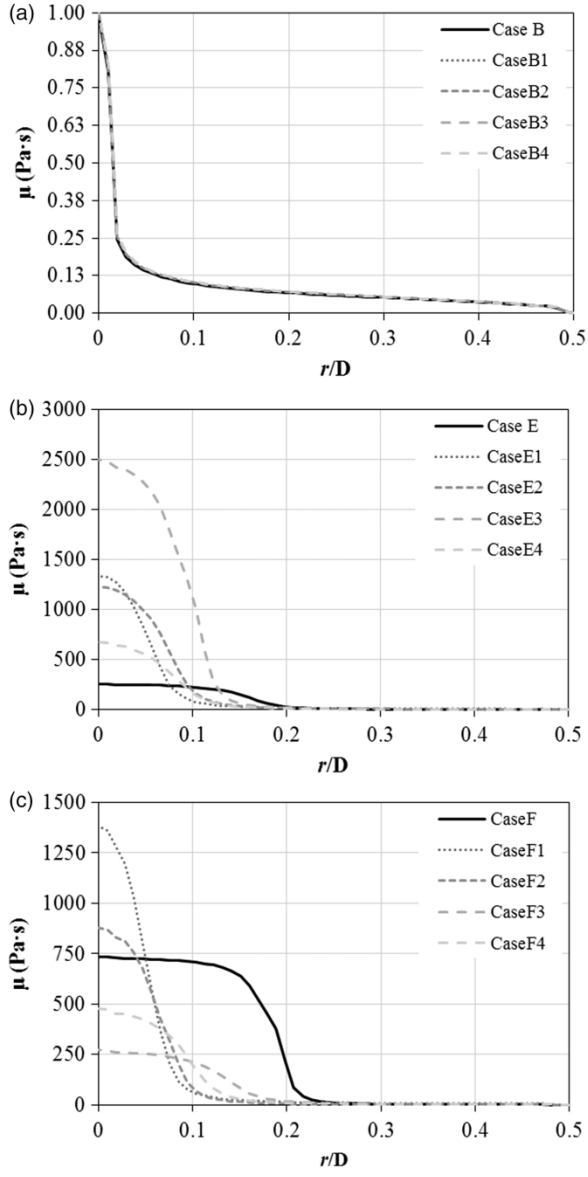

Figure 12. Numerical dynamic viscosity profiles obtained for (a) cases B, B1 to B4 (c = 1.50%(w/w), U_{in} = 6.61 m·s^{-1}), (b) cases E, E1 to E4 (c = 2.50%(w/w), U_{in} = 4.90 m·s^{-1}), and, (c) cases F, F1 to F4 (c = 2.50%(w/w), U_{in} = 5.55 m·s^{-1}).

differences are quite evident (Figures 12b) and c)). Moreover, for cases E4 and F4 viscosity is not only lower than for the *standard* Jäsberg parameters but, additionally, the higher viscosities do not prevail to so close to the wall, this justifying the lower pressure drop values obtained. For cases E4, F2 and F4 it is also observed a decrease on turbulence (Figure 13) and it can be concluded that the parameters α and β have a strong impact on the numerical results. The numerical turbulent kinetic energy has the maximum decrease, compared to the standard cases (cases B, E and F), when the yield region has a lower thickness and the core region has a higher thickness (the slope of the core region is lower (increase of β) and the slope of the yield region is higher (increase of α)). This agrees with what was to be expected since a larger plug of fibers should lead to turbulence damping. Comparing cases B with cases F, pulp consistency is higher and mean inlet velocity is lower in cases F, thus, the more concentrated suspension (cases F) has a higher resistance to the flow and therefore a lower-velocity gradient is observed in the core region.

5. Summary and perspectives

In the present paper a numerical study of *Eucalyptus* pulp flow in a pipe was developed using the commercial CFD software, ANSYS FLUENT 13.0. The CFD code was modified by considering the non-Newtonian behavior of the pulp introduced into the CFD model by viscosity dependence on the local shear rate. The developed model was also modified by considering the logarithmic wall function expression following the proposal of Jäsberg (2007).

The drag-reduction effect was reproduced for various fiber consistencies and flow bulk velocities with the different sets of Jäsberg adjustable parameters. For the highest pulp consistency, the dynamic viscosity has a highest gradient near the pipe wall. For these cases, the existence of the yield and the core regions in the dimensionless velocity profile is more evident. For the cases where the pulp

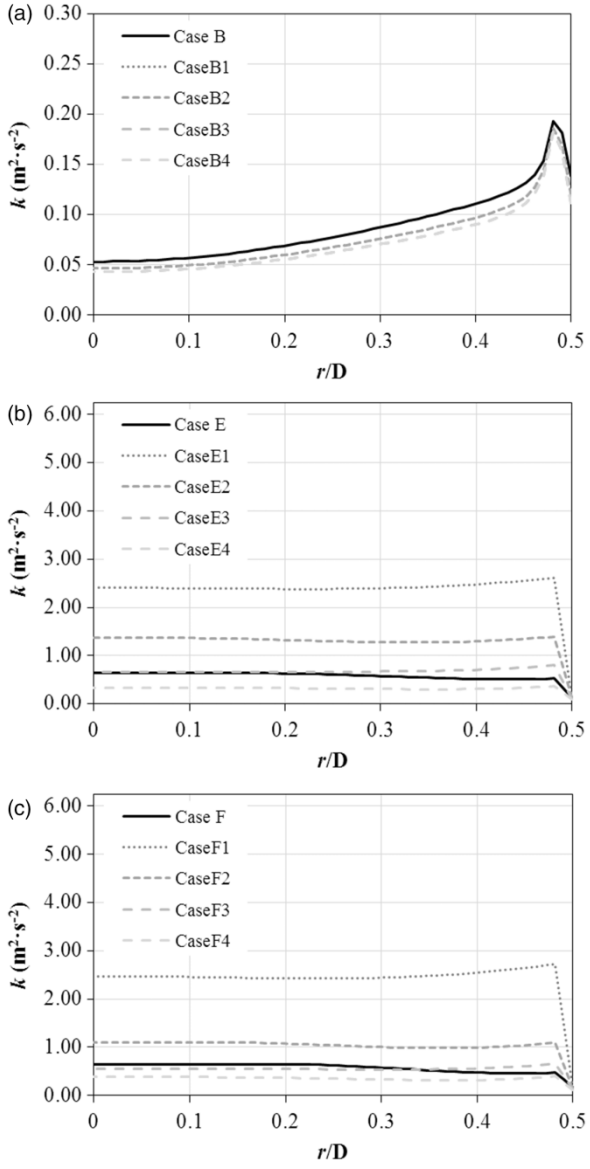

Figure 13. Numerical turbulent kinetic energy obtained for (a) cases B, B1 to B4 (c = 1.50%(w/w), U_{in} = 6.61 m·s^{-1}), (b) cases E, E1 to E4 (c = 2.50%(w/w), U_{in} = 4.90 m·s^{-1}), and, (c) cases F, F1 to F4 (c = 2.50%(w/w), U_{in} = 5.55 m·s^{-1}).

consistency was equal to 2.50% (w/w), the core region has a higher thickness and the *standard* Jäsberg adjustable parameters are not adequate. The slope in the yield region increases and the thickness and the corresponding slope in the core region are reduced. Thus, the Jäsberg parameter α corresponding to the yield region has to increase and the same must happen to the parameter β associated with the core region, this meaning that its slope decreases. A better fit to the experimental pressure drop is obtained in this case. A better fit between calculated and experimental pressure drop is always obtained when the simulated and the calculated Jäsberg dimensionless velocity profiles are similar, what means that the quantitative agreement can only be achieved providing the qualitative correspondence between model and reality exists.

In summary, the strategy followed in this work is able to predict the turbulent flow of concentrated pulp suspensions, but in a future work, it is foreseen to extend the numerical model by considering the presence of fibers in the near-wall region, as shown experimentally by Olson (1996) and predicted by LES simulations of Dong et al. (2003), since that will affect the local viscosity and in turn the transfer of momentum and turbulence in the near-wall region and finally the flow resistance expressed as pressure drop.

Acknowledgements

The present work was developed under the project PTDC/QUE-QUE/112388/2009 and Pest/C/EQB/UI0102/2013, financed by FCT/MCTES (PIDDAC) and co-financed by the European Regional Development Fund (ERDF) through the program COMPETE (POFC) and in connection with COST Action FP1005.

Nomenclature

B	constant in Equation (13) [-]
c	pulp consistency [% (w/w)]
$C_{\varepsilon 1}, C_{\varepsilon 2}, C_{\mu}$	turbulence model constants [-]
D	pipe diameter [m]
k	turbulent kinetic energy [m^2·s^{-2}]
K	consistency coefficient [Pa·s^n]
L	pipe length [m]
n	local coordinate normal to the wall [m]
n	flow behavior index [-]
p	pressure [Pa]
r	radial coordinate [m]
Re_W	Reynolds number based on the viscosity near the wall, ate the interface with the water annulus
R^+	dimensionless radius of the core region
u	axial velocity component [m·s^{-1}]
U_{in}	mean inlet pulp flow velocity [m·s^{-1}]
u^+	dimensionless velocity [-]
V	bulk velocity [m·s^{-1}]
v	radial velocity component [m·s^{-1}]
x	axial coordinate [m]
y_P	distance from point P to the wall [m]
y^+	dimensionless distance to the pipe wall [-]
y_C^+	dimensionless variable position of the plug surface [-]
y_L^+	dimensionless distance between the near wall region and the yield region [-]

Greek letters

$\Delta P/L$	pressure drop [Pa·m^{-1}]
Δu^+	additional term on dimensionless velocity equation (Equation (13)) [-]
α	indicator of the slope in relation to Newtonian profile value of the envelope curve in the yield region [-]
β	indicator of the slope in relation to Newtonian profile value of the envelope curve in the core region [-]
$\dot{\gamma}$	shear rate [s^{-1}]
δ	relative error [%]
ε	dissipation rate of turbulent kinetic energy [m^2·s^{-3}]
κ	von Kármán constant [-]

μ	dynamic viscosity of suspension [Pa·s]
μ_{app}	apparent viscosity of suspension [Pa·s]
μ_t	turbulent viscosity [-]
ρ	pulp density [kg·m^{-3}]
σ_k, σ_ε	turbulence model constants [-]
τ	shear stress [N·m^{-2}]
τ_w	wall shear stress [N·m^{-2}]

References

ANSYS FLUENT Documentation, Ansys Fluent 14.0. 2011.

Asendrych, D., & Kondora, G. (2009, June 1–4). *Fibre suspension mixing in hydropulper chest*. Proceedings of the Papermaking Research Symposium. Kuopio, Finland.

Blanco, A., Negro, C., Fluente, E., & Tijero, J. (2007). Rotor selection for a Searle-type device to study the rheology of paper pulp suspensions. *Chemical Engineering and Processing*, *46*(1), 37–44.

Chang, K. C., Hsieh, W. D., & Chen, C. S. (1995). A modified low-Reynolds-number turbulence model applicable to recirculating flow in pipe expansion. *Journal of Fluids Engineering*, *117*(3), 417–423.

Derakhshandeh, B., Kerekes, R. J., Hatzikiriakos, S. G., & Bennington, C. P. J. (2011). Rheology of pulp fibre suspensions: a critical review. *Chemical Engineering Science*, *66*(15), 3460–3470.

Dong, S., Feng, X., Salcudean, M., & Gartshore, I. (2003). Concentration of pulp fibres in 3D turbulent channel flow. *International Journal of Multiphase Flow*, *29*(1), 1–21.

Fang, J., Ling, X., & Sang, Z. F. (2013). Solid suspension in stirred tank equipped with multi-side-entering agitators. *Engineering Applications of Computational Fluid Mechanics*, *7*(2), 282–294.

Ferziger, J. H., & Peric, M. (2002). *Computational methods for fluid dynamics*. Berlin Heidelberg: Springer-Verlag.

Fock, H., Wiklund, J., & Rasmuson, A. (2009). Ultrasound velocity profile (UVP) measurements of pulp suspensions flow near the wall. *Journal of Pulp and Paper Science*, *35*(1), 26–33.

Galván, S., Reggio, M., & Guibault, F. (2011). Assessment study of *k-ε* turbulence models and near-wall modeling for steady state swirling flow analysis in draft tube using *FLUENT*. *Engineering Applications of Computational Fluid Mechanics*, *5*(4), 459–478.

Gullichsen, J., & Härkönen, E. (1981). Medium consistency technology. *TAPPI Journal*, *64*(6), 69–72.

Hämäläinen, J., Lindström, S. B., Hämäläinen, T., & Niskanen, H. (2011). Papermaking fibre-suspension flow simulations at multiple scales. *Journal of Engineering Mathematics*, *71*(1), 55–79.

Hammarström, D. (2004). *A model for simulation of fiber suspension flows* (BSc thesis). KTH Royal Institute of Technology.

Hsieh, W. D., & Chang, K. C. (1996). Calculation of wall heat transfer in pipe-expansion turbulent flows. *International Journal of Heat and Mass Transfer*, *39*(18), 3813–3822.

Huhtanen, J. P., & Karvinen, R. J. (2005). Interaction of non-newtonian fluid dynamics and turbulence on the behaviour of pulp suspension flows. *Annual Transactions of the Nordic Rheology Society*, *13*, 177–186.

Huhtanen, J. P., & Karvinen, R. J. (2006). Characterisation of non-Newtonian fluid models for wood fibre suspensions in laminar and turbulent flows. *Annual Transactions of the Nordic Rheology Society*, *14*, 51–60.

Jäsberg, A. (2007). *Flow behaviour of fibre suspensions in straight pipes: new experimental techniques and multiphase modelling* (PhD thesis). University of Jyväskylä.

Kondora, G., & Asendrych, D. (2013). Flow modelling in a low consistency disc refiner. *Nordic Pulp & Paper Research Journal*, *28*(1), 119–130.

Li, A., Green, S., & Franzen, M. (2001). *Optimum consistency for pumping pulp*. Technical Information Paper TAPPI TIP 0410-15.

Lundell, F., Söderberg, L. D., & Alfredsson, P. H. (2011). Fluid mechanics of papermaking. *Annual Review of Fluid Mechanics*, *43*, 195–217.

Mathur, A., & He, S. (2013). Performance and implementation of the Launder-Sharma low-Reynolds number turbulence model. *Computers & Fluids*, *79*(25), 134–139.

Olson, J. S. (1996). *The effect of fibre length on passage through narrow apertures* (PhD thesis). University of British Columbia.

Rudman, M., & Blackburn, H. M. (2006). Direct numerical simulation of turbulent non-Newtonian flow using a spectral element method. *Applied Mathematical Modelling*, *30*(11), 1229–1248.

Vatani, A., & Mohammed, H. A. (2013). Turbulent nanofluid flow over periodic rib-grooved channels. *Engineering Applications of Computational Fluid Mechanics*, *7*(3), 369–381.

Ventura, C., Blanco, A., Negro, C., Ferreira, P., Garcia, F., & Rasteiro, M. (2007). Modeling pulp fiber suspension rheology. *TAPPI Journal*, *6*(7), 17–23.

Ventura, C., Garcia, F., Ferreira, P., & Rasteiro, M. (2008). Flow dynamics of pulp fiber suspensions. *TAPPI Journal*, *7*(8): 20–26.

Ventura, C. A. F., Garcia, F. A. P., Ferreira, P. J., & Rasteiro, M. G. (2011). Modeling the turbulent flow of pulp suspensions. *Industrial & Engineering Chemistry Research*, *50*(16), 735–742.

Xu, H., & Aidun, C. (2005). Characteristics of fibre suspension flow in a rectangular channel. *International Journal of Multiphase Flow*, *31*(3), 318–336.